

UCLA

UCLA Previously Published Works

Title

An Initiation Kinetics Prediction Model Enables Rational Design of Ruthenium Olefin Metathesis Catalysts Bearing Modified Chelating Benzylidenes

Permalink

<https://escholarship.org/uc/item/81w2x10v>

Journal

ACS Catalysis, 8(5)

ISSN

2155-5435

Authors

Luo, Shao-Xiong Lennon
Engle, Keary M
Dong, Xiaofei
[et al.](#)

Publication Date

2018-05-04

DOI

10.1021/acscatal.8b00843

Peer reviewed



Published in final edited form as:

ACS Catal. 2018 May 4; 8(5): 4600–4611. doi:10.1021/acscatal.8b00843.

An Initiation Kinetics Prediction Model Enables Rational Design of Ruthenium Olefin Metathesis Catalysts Bearing Modified Chelating Benzylidenes

Shao-Xiong Luo^{†,∇}, Keary M. Engle^{†,¶}, Xiaofei Dong^{||}, Andrew Hejl^{†,‡}, Michael K. Takase[†], Lawrence M. Henling[†], Peng Liu[§], K. N. Houk^{||}, Robert H. Grubbs[†]

[†]Arnold and Mabel Beckman Laboratories of Chemical Synthesis, California Institute of Technology, Pasadena, California 91125, United States

[§]Department of Chemistry, University of Pittsburgh, Pittsburgh, Pennsylvania 15260, United States

^{||} Department of Chemistry and Biochemistry, University of California, Los Angeles, California 90095, United States

Abstract

Rational design of second-generation ruthenium olefin metathesis catalysts with desired initiation rates can be enabled by a computational model that depends on a single thermodynamic parameter. Using a computational model with no assumption about the specific initiation mechanism, the initiation kinetics of a spectrum of second-generation ruthenium olefin metathesis catalysts bearing modified chelating *ortho*-alkoxy benzylidenes were predicted in this work. Experimental tests of the validity of the computational model were achieved by the synthesis of a series of ruthenium olefin metathesis catalysts and investigation of initiation rates by UV/Vis kinetics, NMR spectroscopy, and structural characterization by X-ray crystallography. Included in this series of catalysts were thirteen catalysts bearing alkoxy groups with varied steric bulk on the chelating benzylidene, ranging from ethoxy to dicyclohexylmethoxy groups. The experimentally observed initiation kinetics of the synthesized catalysts were in good accordance with computational predictions. Notably, the fast initiation rate of the dicyclohexylmethoxy catalyst was successfully predicted by the model, and this complex is believed to be among the fastest initiating Hoveyda–Grubbs-type catalysts reported to date. The compatibility of the predictive model with other catalyst families, including those bearing alternative NHC ligands or disubstituted alkoxy benzylidenes, was also examined.

Corresponding Author: pengliu@pitt.edu, houk@chem.ucla.edu, rhg@caltech.edu.

[∇]Department of Chemistry, Massachusetts Institute of Technology, 77 Massachusetts Ave., Cambridge, Massachusetts 02139, United States

[¶]The Scripps Research Institute, Department of Chemistry, 10550 N. Torrey Pines Rd., La Jolla, California 92037, United States

[‡]Dow Coating Materials, The Dow Chemical Company, 400 Arcola Rd., Collegetown, Pennsylvania 19426, United States

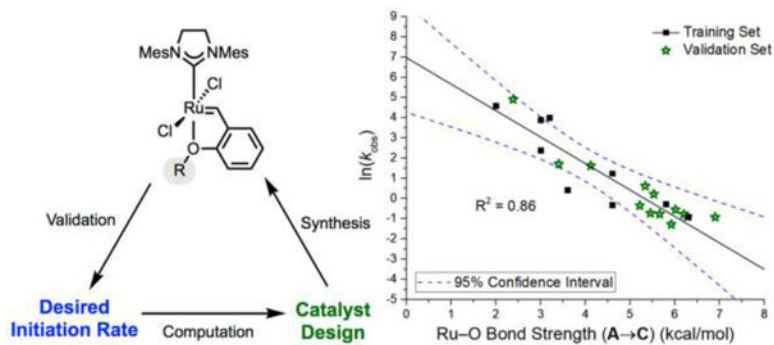
ASSOCIATED CONTENT

Supporting Information

Experimental details, NMR spectra of new compounds, CIFs of catalysts, optimized Cartesian coordinates and energies, details of computational methods. This material is available free of charge via the Internet at <http://pubs.acs.org>.

The authors declare no competing financial interest.

Graphical Abstract



INTRODUCTION

Olefin metathesis is a powerful method to form carbon–carbon double bonds¹ with control of regio-² and stereoselectivity.³ There are extensive applications of cross metathesis (CM), ring closing metathesis (RCM) and ring-opening metathesis polymerization (ROMP) for a variety of purposes, ranging from natural product synthesis⁴ to chemical feedstock conversion⁵ to advanced materials synthesis.⁶ One of the major milestones in the development of olefin metathesis as a synthetic method was the discovery of well-defined ruthenium–alkylidene catalysts,⁷ which demonstrated superior tolerance towards moisture, air and functional groups compared to early transition metal catalysts.

Figure 1 shows a collection of commonly used ruthenium-based olefin metathesis catalysts. Each type of catalyst is unique in its reactivity and selectivity profile and hence has unique olefin metathesis applications. For example, catalysts **6** and **7** are especially fast-initiating and suitable for catalyzing ROMP to give polymers with high molecular weight and low dispersity.⁸ Catalyst **5**, discovered by Hoveyda and Blechert,⁹ is well known for its stability and tolerance to air, moisture, and Lewis basic functional groups. The chelation of the *ortho*-alkoxy benzylidene to the ruthenium center at the axial site results in the exceptional stability of **5** and its derivatives, making them valuable tools for organic synthesis.^{1a, 1b, 10} Another advantage of catalyst **5** is the absence of the labile phosphine ligands which are responsible for certain phosphine-mediated catalyst decomposition pathways.¹¹

The initiation kinetics of an olefin metathesis catalyst have significant impact on its reactivity and hence its applications.^{1a, 1b, 10a, 12} Since the initiation mechanism for Hoveyda–Grubbs-type catalysts is an ongoing topic of investigation,¹³ it is valuable to establish a model to correlate initiation kinetics with thermodynamic parameters in a manner that avoids making assumptions of the initiation mechanism. In a previous report, we systematically investigated a series of ruthenium-based olefin metathesis catalysts bearing modified chelating *ortho*-alkoxy/aryloxybenzylidenes (Figure 2).¹⁴ It was shown that by tuning the structure of the alkoxy/aryloxy group, catalysts with a wide range of initiation rates could be accessed. More importantly, a computational model that makes no specific assumptions regarding the initiation mechanism was proposed and was tested versus the initiation rates of the catalysts studied. This model established a good correlation between

the computed reaction energy of initiation with butyl vinyl ether (BVE) to form a common 14-electron Fischer carbene complex **C** ($G_r(\mathbf{A} \rightarrow \mathbf{C})$) and the experimental initiation rate of the catalyst (Figure 3). The correlation is given by Equation 1. In the present work, this model is employed to predict the initiation kinetics of new catalysts, and these predictions are then tested experimentally.

RESULTS AND DISCUSSION

Catalyst Design.

Having previously established the aforementioned computational model with an initial training set, we next sought to use this model to extrapolate and predict the initiation rates of other ruthenium-based olefin metathesis catalysts bearing modified chelating *ortho*-alkoxy benzylidenes. To this end, a wide variety of Hoveyda–Grubbs type olefin metathesis catalysts were considered (**16–38**). Catalyst **20**, **23** and **25** are known catalysts,¹⁵ yet their initiation rates have not been previously measured. As analogues to the standard *i*-Pr control, catalysts **16–19** were proposed to examine the effect of increasing steric bulk from ethoxy to *tert*-butoxy. Catalysts **20** and **21** were considered to evaluate the effect of the distance of the phenyl ring on the initiation rates as compared to catalyst **11** discovered by Plenio and coworkers.¹⁶ This series of alkoxy-modified Hoveyda–Grubbs variants also includes cycloalkyl groups of various ring sizes, from cyclobutyl to cyclooctyl groups (**22–26**). They provide a direct comparison with the cyclopropyl catalyst (**12**), which was included in the original training set. Dicyclohexylmethoxy (**27**) catalyst was intended to mimic the parent *i*-Pr catalyst, but with substantially greater steric bulk.¹⁷ Similar to the rationale in proposing catalysts **20** and **21**, catalyst **28** was included to probe the impact of additional methylene spacer at the 1-adamantyl position compared with catalyst **14**. As catalyst **15** was discovered to be fast-initiating in our previous report,¹⁴ we hoped to enhance the initiation rate even further by introducing an additional methyl group at the 2-adamantyl position. It is also interesting to examine how well the model is able to predict the initiation properties of catalysts bearing electron-withdrawing groups attached to oxygen,^{12g, 15a} such as a trifluoromethyl group (**30–31**). To further evaluate the scope of the computational model, we also examined the known 2,6-dimethoxy analogue (**32**)^{12e, 18} of catalyst **10**. In particular, we were interested to investigate the relationship between OMe-exchange and initiation in this catalyst. Lastly, we sought to test the scope of the computational model by examining catalysts with modified *N*-heterocyclic carbene (NHC) ligands. As common variants of the standard SIMes NHC ligand, SIPr¹⁹ and SITol²⁰ NHC ligands were used, and a series of catalysts bearing these two ligands and chelating benzylidenes with different steric bulk at the alkoxy position was prepared (**33 – 38**).

Computed Ru–O Bond Energies and Predicted Initiation Rates.

The computational method used for the proposed catalysts is consistent with previous computational studies.^{14,21} The strengths of Ru–O bonding interactions were evaluated in two ways (Figure 3): (1) by calculating the energy difference between the nonchelated 14-electron complex **B** formed by dechelation of the Ru–O bond and rotation of the *o*-alkoxyphenyl group and the ground-state chelated conformation **A** ($G_r(\mathbf{A} \rightarrow \mathbf{B})$) and (2) by calculating the reaction energy to form a common 14-electron Fischer carbene complex **C**

from the ground-state chelated conformation **A** and BVE ($G_r(\mathbf{A} \rightarrow \mathbf{C})$). The geometries were optimized in the gas phase using B3LYP with a mixed basis set of LANL2DZ for ruthenium and 6-31G(d) other atoms. Energies were calculated with M06 single-point calculations with a mixed basis set of SDD for ruthenium and 6-311+G(d,p) for other atoms using the SMD solvation model in toluene. B3LYP, BP86, M06, M06-L and ω B97x-D have been previously employed to optimize the geometries; B3LYP and BP86 were found to produce better correlation between the computed Ru–O bond strengths and the observed initiation rate ($\ln(k_{\text{obs}})$) than the others.¹⁴

Computed Ru–O bond strengths derived from both methods ($G_r(\mathbf{A} \rightarrow \mathbf{B})$ and $G_r(\mathbf{A} \rightarrow \mathbf{C})$) are summarized in Table 1. The initiation rates of the proposed catalysts (**16–38**) were predicted by Equation 1 with the calculated $G_r(\mathbf{A} \rightarrow \mathbf{C})$ values. In order to clearly compare and contrast the computational results, the calculated $G_r(\mathbf{A} \rightarrow \mathbf{C})$ values for catalysts bearing SIMes NHC ligand are presented in Figure 4, and the results with catalysts bearing non-SIMes NHC ligands are shown in Figure 5. It should be noted that, except for the ethoxy catalyst **16**, all proposed catalysts have a $G_r(\mathbf{A} \rightarrow \mathbf{C})$ value lower than the *i*-Pr control (entry 1, Table 1), hence they are predicted to initiate faster than **5**. In particular, the calculated $G_r(\mathbf{A} \rightarrow \mathbf{C})$ values for **27** and **29–31** are significantly lower than others, which is attributed to steric clashing between the bulky alkoxy group (dicylohexylmethoxy or 2-methyl-2-adamantyloxy) and the SIMes-dichlororuthenium fragment and to the strong electron-withdrawing effect of the trifluoromethyl group in weakening Ru–O coordination and destabilizing the catalysts. The benzyl catalyst (**20**) is predicted to initiate faster than the phenethyl catalyst (**21**), as the phenyl ring is closer to the ruthenium center in **20**. Moreover,

$G_r(\mathbf{A} \rightarrow \mathbf{C})$ values for catalysts bearing larger cycloalkyl rings (**24–26**) are not significantly smaller than those of catalysts with smaller ring sizes (**22–23**) due to the structural flexibility of the rings. Consistent with the results from a recent computational study by Trzaskowski et al.,²² catalysts **22** and **23** are predicted to initiate with similar rates as the isopropyl control **5**. It is also surprising to see that the calculated $G_r(\mathbf{A} \rightarrow \mathbf{C})$ values for catalysts bearing non-SIMes NHC ligands (**33–38**) remain relatively constant across the different alkoxy groups (Figure 5). The introduction of the 2-Ada group is expected to significantly decrease the $G_r(\mathbf{A} \rightarrow \mathbf{C})$ value, yet this is not borne out in the computational data for complexes **33–38**. This data further motivated us to experimentally investigate the initiation kinetics of **33–38** in order to shed light on to the scope and limitations of the current model.

Synthesis of catalysts.

The synthesis of the proposed catalysts and their precursors followed reported procedures.^{14, 23} 2-Alkoxy-benzaldehyde intermediates were synthesized from 2-fluorobenzaldehyde and the respective alcohols via a three-step S_NAr procedure (Scheme 1). The resulting benzaldehydes were converted to the respective styrenes by Wittig olefination.

Three different synthetic procedures (Methods A–C) were employed for the final step to introduce the chelating benzyldene group onto the complex. A summary of methods and yields for the synthesis of **16–38** (except for commercially available complexes **33** and **36**) is shown in Table 2. Most of the proposed catalysts were synthesized in moderate to high

yields. Consistent with the observation in our previous study,¹⁴ Method C was found to be more effective in synthesizing the more sterically demanding catalyst **27** (entry 12, Table 2). Notably, attempts to synthesize catalysts **29–31** were unsuccessful, possibly due to weak Ru–O bonding from electronic (**30–31**) or steric (**29**) perturbation on the alkoxy group, as predicted by the DFT calculations. This observation is consistent with the unsuccessful attempts by Barbasiewicz and coworkers to obtain **30** by lowering the temperature or terminating the reaction at lower conversion.^{15a} For catalyst **32**, Method B under extended reaction time was effective, whereas Method C was found to be incompatible (entry 17, Table 2).

X-ray Crystal Structures.

Single crystals suitable for X-ray diffraction were grown and analyzed for all newly synthesized catalysts.²⁴ Graphical representations of the single crystal structures are summarized in Figure 6, confirming the expected connectivity of the catalysts. The series includes commercially available catalyst **33** (the structure of which had not been previously reported). The X-ray structures of **32** and **35** have been previously reported.^{18a, 20} Catalysts **17–18**, **21**, **24–25**, **26** and **32** crystallized in the space group $P2_1/n$, while catalysts **20**, **28** and **34** crystallized in the space group $P2_1/c$. Catalysts **22**, **33** and **35** crystallized in the space group $\bar{P}1$, and catalysts **16** and **23** crystallized in the space group $C2/c$. Catalyst **19** crystallized in the space group $Pbcn$. Catalysts **27** and **38** crystallized in the space group $Pbca$. Catalyst **37** crystallized in the space group $P2_12_12_1$. Two crystallographically inequivalent conformers were found in the unit cell for catalysts **18**, **22**, **26** and **33**, and in these cases the quoted bond lengths represent the average of the values of the two conformers. In general, there is no apparent correlation between the Ru–O bond length and the size of the alkoxy substituent; the Ru–O and Ru=C bond lengths (Table 3) are observed to be fairly constant for most of the catalysts in the series, with the exception of **27** (entry 12, Table 3), **35** (entry 17, Table 3), and **38** (entry 20, Table 3), whose Ru–O bonds are exceptionally long. Similar to the X-ray structure for catalyst **15**,¹⁴ elongation of the Ru–O bonds serves to accommodate the energetically unfavorable steric clash between the SIMes-dichlororuthenium fragment and a methylene unit on the 2-Ada group (**35** and **38**) or the dicyclohexyl group (**27**).

NMR Spectra.

The series of newly synthesized catalysts was next studied by ¹H and ¹³C NMR spectroscopy in CD₂Cl₂. The characteristic benzylidene peaks of the catalysts were observed to be in the 16–17 ppm (¹H) and 280–290 ppm (¹³C) ranges. Detailed results are summarized in Table 4. Chemical shifts of the carbenes on the NHC ligands, which are typically observed at 210 ppm (¹³C), are also compiled in Table 4. There seems to be no definitive trend between the NMR shifts of the benzylidene moiety and the size of the alkoxy group.

Initiation Rates by UV/Vis Kinetics Studies.

To test the validity of the predictions made by the computational model, the initiation rates of the synthesized catalysts were measured experimentally by UV/Vis spectrometry. We

have previously found that results from this assay are in good agreement with initiation rates of a representative catalytic RCM reaction.¹⁴ Following identical procedures as in our previous report, initiation rates were determined by reacting the catalysts (10^{-4} M) with a large excess of butyl vinyl ether (BVE) (30 equiv) at 10 °C under pseudo-first-order conditions. The observed initiation rates were calculated based on the decay of the λ_{max} peak by UV/Vis spectrometry as the catalysts reacted with BVE. Detailed results are summarized in Table 5, and the relative rate with respect to catalyst **5** (k_{rel}) was also calculated. A large range of initiation rates were observed throughout the series of catalysts. Taking the *i*-Pr catalyst as control (entry 1, Table 5), k_{rel} values of the catalysts span four orders of magnitude, ranging from 0.69 (**22**, entry 3, Table 5) to 340 (**27**, entry 15, Table 5). The increase in initiation rate tracks closely with increasing steric bulk at the alkoxy position. In particular, dicyclohexylmethoxy catalyst **27** was found to initiate the fastest in the entire series, consistent with the prediction from the computational model. In fact, **27** initiates faster than the well-known fast-initiating Blechert (**8**) and Plenio (**11**) catalysts with BVE at 10 °C.²⁵ The single-crystal X-ray structure of **27** (Figure 6) shows that one of the cyclohexyl rings is positioned in an energetically unfavorable pseudo-axial conformation, thus lowering the energy barrier to access the catalytically active non-chelated 14-electron complex. The unfavorable energy profile of the chelated form of catalyst **27** is also reflected in the low yield of its preparation using method C (47%, entry 12, Table 2), which was typically found to be effective for the chelation of more challenging styrenes.¹⁴ The fast-initiating properties of **27** are also consistent with the exceptionally long Ru–O bond length found in its X-ray structure (2.394 Å, entry 12, Table 3). Consistent with the computed results, the catalysts with larger cycloalkyl groups such as cyclooctyl (**26**, entry 7, Table 5) and cycloheptyl (**25**, entry 5, Table 5) rings do not initiate significantly faster than the catalysts with smaller cycloalkyl groups like cyclobutyl (**22**, entry 3, Table 5) or cyclopentyl (**23**, entry 9, Table 5). Again, this observation is attributed to the flexible ring structures that have limited contribution to the steric bulk of the alkoxy group and hence insignificant impact on initiation rates. Benzyl catalyst (**20**, entry 13, Table 5) was found to initiate 10 times faster than the phenethyl analogue (**21**, entry 6, Table 5), an effect that could be steric or electronic in nature. In comparing the crystal structures of **20** and **21** (Figure 6), one can see that the benzyl group of **20** is situated perpendicular to the mesityl ring on the NHC ligand, whereas the phenyl ring in **21** is parallel to the mesityl ring and pointing away from the SIMes-dichlororuthenium fragment, suggesting potential edge-to-face and face-to-face π -stacking respectively. It should also be noted that the 2,6-diOMe catalyst **32** was observed to initiate only at elevated temperatures (55 °C),¹⁸ possibly due to rapid exchange of the methoxy groups, a phenomenon that merited further investigation.

Variation of the NHC ligand also had a significant impact on the initiation rates of the catalysts. Catalysts bearing the SIPr NHC ligand (**33–35**, entries 16–18, Table 5) were found to initiate much slower than their SIMes counterparts, consistent with the observations reported by Percy and coworkers,²⁶ whereas catalysts with the SITol NHC ligand (**36–38**, entries 19–21, Table 5) were found to initiate with comparable rates. Notably, across the NHC ligand series, there was a consistent trend of faster initiation rate with increasing steric bulk on the alkoxy group from *i*-Pr (**5**, **33**, **36**) to 1-Ada (**14**, **34**, **37**) to 2-Ada groups (**15**, **35**, **38**) (Table 6). In particular, fast-initiating catalysts such as **38** and **27** initiate about 2000 and

3600 times faster than **33**, respectively. This observation is another demonstration of the synergistic power of tuning the alkoxy group and the NHC ligand together to access catalysts with a broad range of initiation rates.

Validity of Computational Model in Predicting Experimental Initiation Rates.

Predicted initiation kinetics of the synthesized catalysts are tabulated and compared against the experimental values from the UV/Vis kinetics experiments (Table 7). To better illustrate the comparison and evaluate the accuracy of the initiation-prediction model, scatter plots of the SIMes catalysts series (Figure 7) and SIPr and SITol series (Figure 8) are shown. The experimental results are illustrated as colored points on the scatterplot (SIMes: green stars; SIPr and SITol: red circles), whereas the solid black line represents the predicted trend given by Equation 1. To gauge the deviation of the experimental initiation rates from the predicted trend line, dashed blue lines are plotted around the predicted trend line to show the 95% confidence band derived and extrapolated from the training set (**5** and **8–15**) in the prediction model.

As shown in Figure 7, all of the experimental initiation rate values fall within the 95% confidence prediction band of the prediction model. This indicates that the model provides a reasonably accurate prediction of the initiation kinetics for the newly synthesized catalysts. Notably, catalysts **21** (phenethyl, entry 4, Table 7) and **25** (*c*-heptyl, entry 3, Table 7) are predicted to have very similar initiation rates despite their significantly different steric and electronic properties, and this prediction is borne out experimentally. Considering the fact that the initiation-prediction model is derived from a single-variable linear regression with an R-squared value of 0.79 (Equation 1), the new experimental results ($R^2 = 0.86$ with respect to the solid prediction trendline) are in well accordance with the prediction model.

However, for the catalysts bearing different NHC ligands, as illustrated in Figure 8, the initiation-prediction model shows poor accuracy as illustrated by the large deviation of the experimental values from the predicted trend line ($R^2 = 0.16$). Many contradictory results are observed (Table 7). In particular, catalysts **33** and **35** are predicted to have essentially the same initiation rates, yet the experimental results show that **35** initiates about 80 times faster. Similarly, catalyst **34** is predicted to initiate faster than **38**, but the experimental results show that **38** is actually about 760 times faster. This suggests that the current initiation-prediction model, which was developed based on catalysts bearing the SIMes NHC ligand, cannot be extended to catalyst bearing the SIPr and SITol NHC ligands. Future directions include developing a new prediction model (or collection of models) to accommodate different NHC ligands. Moreover, although catalysts **29–31** are too unstable to be synthesized, their computed Ru–O bond strengths can be valuable in identifying the limits of Ru–O chelation in the current initiation-prediction model. This boundary condition can serve as a convenient indication of structural stability in the future design of fast-initiating catalysts.

In our previous report,¹⁴ the computed Ru–O bond strength from the dechelation process ($G_r(\mathbf{A} \rightarrow \mathbf{B})$) was found to be a poor predictor for catalyst initiation kinetics. This relationship was reevaluated with the new data from the catalysts synthesized in this study. Again, the computed Ru–O bond strength from $G_r(\mathbf{A} \rightarrow \mathbf{B})$ shows weak correlation with

the observed initiation rates ($R^2 = 0.50$, Figure 9), recapitulating that the use of $G_r(\mathbf{A} \rightarrow \mathbf{C})$ is superior to using $G_r(\mathbf{A} \rightarrow \mathbf{B})$ in Ru–O bond strength estimation for initiation kinetics studies.²⁷

Chelate Dissociation Rate versus Initiation Rate.

It is especially interesting to investigate the initiation kinetics of the 2,6-diOMe catalyst **32** because the 2,6-dimethoxy group on the benzylidene chelate provides an opportunity to study the chelate dissociation rate of Grubbs–Hoveyda olefin metathesis catalysts.

Even though catalyst **32** is predicted to have similar initiation kinetics as catalyst **22** or **26**, it did not initiate at 10 °C like the rest of the catalysts in the series (entry 2, Table 5). Nevertheless, it was previously shown to catalyze ring-closing metathesis (RCM) reaction at elevated temperature.¹⁸ We found that even at higher temperature (50–100 °C), the initiation rate of catalyst **32** is too low to obtain an accurate measurement at the concentration typically used for UV/Vis experiments. As such, reaction kinetics were measured by ¹H NMR spectroscopy ($[\text{Ru}]_0 = 5 \text{ mM}$) by subjecting **32** to a large excess of BVE (30 equiv) at 70 °C in *d*₈-toluene.^{12a, 12b} The initiation rate profile of **32** (Figure 10) is obtained by measuring the decay of the benzylidene ¹H NMR peak (17.27 ppm in toluene-*d*₈), and the results are in good accordance with the assumption of pseudo-first-order decay. As the methoxy group in **32** presents less steric bulk and the incoming BVE is relatively electron-rich and sterically non-demanding, the initiation mode of **32** is expected to lean towards the interchange mechanism where the initiation kinetics is dominated by the interchange rate k_1 , which is approximated by $k_{\text{obs}}/[\text{BVE}]$.^{13b}

To gauge the dissociation rate of the Ru–O bond, a series of ¹H–¹H EXSY NMR experiments were performed with **32** using pulse sequences with different mixing times to observe the exchange of the two methoxy groups.²⁸ A representative spectrum is shown in Figure 11. The EXSY spectra allowed for direct observation of methoxy group exchange in **32** at 70 °C in deuterated toluene, and the quantitative rate data for the exchange process was thus obtained.

It is instructive to compare the rate of methoxy group exchange in **32** against its initiation kinetics. At 70 °C in deuterated toluene, the methoxy groups exchange rate in **32** is about 3300 times faster than the catalyst's interchange rate with the incoming olefin during the initiation process (Table 8).²⁹ The rate of Ru–O dissociation is expected to be even higher since the methoxy groups do not necessarily exchange every time the Ru–O bond dissociates. These results shed light on the initiation mechanism of **32**. In particular, the observation that Ru–O dissociation is rapid compared to initiation is inconsistent with a purely dissociative initiation pathway with **32**. Rather, interchange or associative mechanisms are more likely in this case.

CONCLUSION

The initiation rates of a series of ruthenium-based olefin metathesis catalysts bearing modified *ortho*-alkoxy benzylidenes have been predicted by a previously developed computational model. This series of catalysts was investigated using a combination of

organometallic synthesis, NMR spectroscopy, X-ray crystallography and initiation kinetics. The computational model satisfactorily predicts the initiation kinetics of the catalysts bearing the SIMes NHC ligand. A total of fourteen new second-generation Grubbs–Hoveyda catalysts have been synthesized and characterized. Among them, the dicyclohexylmethoxy catalyst **27** was found to be one of the fastest-initiating second-generation Hoveyda–Grubbs olefin metathesis catalysts reported to date. The enhanced initiation rate of **27** was successfully predicted by the computational model. A notable aspect of this model is that it does not make any assumptions about the mechanism of catalyst initiation and relies on a single, easily computed thermodynamic metric. This metric gives simple and generally reliable predictions of olefin metathesis catalyst properties *in silico*. Further improvements of the computational model, such as extensions to other NHC ligands, will ultimately provide a more powerful toolkit for the design of customized catalysts with the desired initiation kinetics.

Supplementary Material

Refer to Web version on PubMed Central for supplementary material.

ACKNOWLEDGMENT

We acknowledge Dr. Bruce S. Brunshwig for assistance with the UV/Vis kinetics experiments, which were carried out at the Molecular Materials Research Center of the Beckman Institute at Caltech. The research described in this manuscript was supported financially by the ONR (Award Number N00014-12-1-0596) and the NIH NIGMS (F32GM108145, postdoctoral fellowship to K.M.E.). The Bruker KAPPA APEXII X-ray diffractometer was purchased via an NSF CRIF:MU award to the California Institute of Technology (CHE-0639094). We thank Materia, Inc. for the generous donation of catalysts **2–5**, **33**, **36**, and **39**. Calculations were performed on supercomputers from the DoD HPCMP Open Research Systems and the Extreme Science and Engineering Discovery Environment (XSEDE), which is supported by the NSF. Dr. Tzu-Pin Lin, Dr. Crystal K. Chu and Dr. Timothy P. Montgomery are acknowledged for helpful discussions and assistance with NMR experiments.

REFERENCES

- (1). (a) Grubbs RH; Wenzel AG; O’Leary DJ; Khosravi E Handbook of Metathesis. Wiley-VCH: Weinheim: Germany, 2015; (b) Grela K Olefin Metathesis: Theory and Practice. John Wiley & Sons, Inc.: 2014; (c) Schuster M; Blechert S Olefin Metathesis in Organic Chemistry. Angew. Chem. Int. Ed 1997, 36, 2036–2056; (d) Hoveyda AH; Zhugralin AR The remarkable metal-catalysed olefin metathesis reaction. Nature 2007, 450, 243–251; [PubMed: 17994091] (e) Schrock RR Recent advances in high oxidation state Mo and W imido alkylidene chemistry. Chem. Rev 2009, 109, 3211–3226; [PubMed: 19284732] (f) Lozano-Vila AM; Monsaert S; Bajek A; Verpoort F Ruthenium-based olefin metathesis catalysts derived from alkynes. Chem. Rev 2010, 110, 4865–4909. [PubMed: 20392041]
- (2). (a) Nolan SP; Clavier H Chemoselective olefin metathesis transformations mediated by ruthenium complexes. Chem. Soc. Rev 2010, 39, 3305–3316; [PubMed: 20593074] (b) Chatterjee AK; Choi TL; Sanders DP; Grubbs RH A general model for selectivity in olefin cross metathesis. J. Am. Chem. Soc 2003, 125, 11360–11370; [PubMed: 16220959] (c) Liu Z; Rainier JD Regioselective ring-opening/cross-metathesis reactions of norbornene derivatives with electron-rich olefins. Org. Lett 2005, 7, 131–133; [PubMed: 15624995] (d) Cannon JS; Grubbs RH Alkene chemoselectivity in ruthenium-catalyzed Z-selective olefin metathesis. Angew. Chem. Int. Ed 2013, 52, 9001–9004; (e) Luo SX; Cannon JS; Taylor BL; Engle KM; Houk KN; Grubbs RH Z-Selective Cross-Metathesis and Homodimerization of 3E-1,3-Dienes: Reaction Optimization, Computational Analysis, and Synthetic Applications. J. Am. Chem. Soc 2016, 138, 14039–14046. [PubMed: 27689541]

- (3). (a) Hoveyda AH Evolution of catalytic stereoselective olefin metathesis: from ancillary transformation to purveyor of stereochemical identity. *J. Org. Chem* 2014, 79, 4763–4792; [PubMed: 24720633] (b) Montgomery TP; Johns AM; Grubbs RH Recent Advancements in Stereoselective Olefin Metathesis Using Ruthenium Catalysts. *Catalysts* 2017, 7, 87; (c) Hartung J; Dornan PK; Grubbs RH Enantioselective olefin metathesis with cyclometalated ruthenium complexes. *J. Am. Chem. Soc* 2014, 136, 13029–13037; [PubMed: 25137310] (d) Nguyen TT; Koh MJ; Mann TJ; Schrock RR; Hoveyda AH Synthesis of E- and Z-trisubstituted alkenes by catalytic cross-metathesis. *Nature* 2017, 552, 347–354. [PubMed: 29293209]
- (4). (a) Nicolaou KC; Bulger PG; Sarlah D Metathesis reactions in total synthesis. *Angew. Chem. Int. Ed* 2005, 44, 4490–4527; (b) Cossy J; Arseniyadis S; Meyer C Metathesis in natural product synthesis: strategies, substrates and catalysts. Wiley-VCH: Weinheim: Germany, 2010; (c) Werrel S; Walker JCL; Donohoe TJ Application of catalytic Z-selective olefin metathesis in natural product synthesis. *Tetrahedron Lett* 2015, 56, 5261–5268; (d) Hughes D; Wheeler P; Ene D Olefin Metathesis in Drug Discovery and Development-Examples from Recent Patent Literature. *Org. Process Res. Dev* 2017, 21, 1938–1962; (e) Williams MJ; Kong J; Chung CK; Brunskill A; Campeau LC; McLaughlin M The Discovery of Quinoxaline-Based Metathesis Catalysts from Synthesis of Grazoprevir (MK-5172). *Org. Lett* 2016, 18, 1952–1955; [PubMed: 27123552] (f) Liu DD; Sun TW; Wang KY; Lu Y; Zhang SL; Li YH; Jiang YL; Chen JH; Yang Z Asymmetric Total Synthesis of Lancifodilactone G Acetate. *J. Am. Chem. Soc* 2017, 139, 5732–5735; [PubMed: 28391693] (g) Cheng-Sanchez I; Garcia-Ruiz C; Guerrero-Vasquez GA; Sarabia F An Olefin Cross-Metathesis Approach to Depudecin and Stereoisomeric Analogues. *J. Org. Chem* 2017, 82, 4744–4757. [PubMed: 28397496]
- (5). (a) Marx VM; Herbert MB; Keitz BK; Grubbs RH Stereoselective access to Z and E macrocycles by ruthenium-catalyzed Z-selective ring-closing metathesis and ethenolysis. *J. Am. Chem. Soc* 2013, 135, 94–97; [PubMed: 23244210] (b) Miyazaki H; Herbert MB; Liu P; Dong X; Xu X; Keitz BK; Ung T; Mkrtumyan G; Houk KN; Grubbs RH Selective ethenolysis with a ruthenium metathesis catalyst: experiment and theory. *J. Am. Chem. Soc* 2013, 135, 5848–5858; [PubMed: 23547887] (c) Mangold SL; Grubbs RH Stereoselective synthesis of macrocyclic peptides via a dual olefin metathesis and ethenolysis approach. *Chem. Sci* 2015, 6, 4561–4569; [PubMed: 26509000] (d) Park CP; Van Wingerden MM; Han SY; Kim DP; Grubbs RH Low pressure ethenolysis of renewable methyl oleate in a microchemical system. *Org. Lett* 2011, 13, 2398–2401. [PubMed: 21456591]
- (6). (a) Schrock RR Synthesis of stereoregular polymers through ring-opening metathesis polymerization. *Acc. Chem. Res* 2014, 47, 2457–2466; [PubMed: 24905960] (b) Suthasupa S; Shiotsuki M; Masuda T; Sanda F Alternating ring-opening metathesis copolymerization of amino acid derived norbornene monomers carrying nonprotected carboxy and amino groups based on acid-base interaction. *J. Am. Chem. Soc* 2009, 131, 10546–10551; [PubMed: 19722629] (c) Weitekamp RA; Atwater HA; Grubbs RH Photolithographic olefin metathesis polymerization. *J. Am. Chem. Soc* 2013, 135, 16817–16820; [PubMed: 24171659] (d) Martinez H; Ren N; Matta ME; Hillmyer MA Ring-opening metathesis polymerization of 8-membered cyclic olefins. *Polym. Chem* 2014, 5, 3507–3532; (e) Dong Y; Matson JB; Edgar KJ Olefin Cross-Metathesis in Polymer and Polysaccharide Chemistry: A Review. *Biomacromolecules* 2017, 18, 1661–1676; [PubMed: 28467697] (f) Sinclair F; Alkattan M; Prunet J; Shaver MP Olefin cross metathesis and ring-closing metathesis in polymer chemistry. *Polym. Chem* 2017, 8, 3385–3398; (g) Jang ES; John JM; Schrock RR Synthesis of cis,syndiotactic-A-alt-B Copolymers from Enantiomerically Pure Endo-2-Substituted-5,6-Norbornenes. *J. Am. Chem. Soc* 2017, 139, 5043–5046. [PubMed: 28355081]
- (7). (a) Nguyen ST; Johnson LK; Grubbs RH; Ziller JW Ring-Opening Metathesis Polymerization (ROMP) of Norbornene by a Group-VIII Carbene Complex in Protic Media. *J. Am. Chem. Soc* 1992, 114, 3974–3975; (b) Nguyen ST; Grubbs RH; Ziller JW Syntheses and Activities of New Single-Component, Ruthenium-Based Olefin Metathesis Catalysts. *J. Am. Chem. Soc* 1993, 115, 9858–9859; (c) Schwab P; Grubbs RH; Ziller JW Synthesis and Applications of RuCl₂(=CHR') (PR₃)₂: The Influence of the Alkylidene Moiety on Metathesis Activity. *J. Am. Chem. Soc* 1996, 118, 100–110; (d) Scholl M; Ding S; Lee CW; Grubbs RH Synthesis and activity of a new generation of ruthenium-based olefin metathesis catalysts coordinated with 1,3-dimesityl-4,5-dihydroimidazol-2-ylidene ligands. *Org. Lett* 1999, 1, 953–956; [PubMed: 10823227] (e) Trnka TM; Grubbs RH The Development of L₂X₂Ru=CHR Olefin Metathesis Catalysts: An

- Organometallic Success Story. *Acc. Chem. Res* 2001, 34, 18–29; [PubMed: 11170353]
- (f) Samojlowicz C; Bieniek M; Grela K Ruthenium-based olefin metathesis catalysts bearing N-heterocyclic carbene ligands. *Chem. Rev* 2009, 109, 3708–3742. [PubMed: 19534492]
- (8). (a) Love JA; Morgan JP; Trnka TM; Grubbs RH A practical and highly active ruthenium-based catalyst that effects the cross metathesis of acrylonitrile. *Angew. Chem. Int. Ed* 2002, 41, 4035–4037; (b) Rahman MA; Lokupitiya HN; Ganewatta MS; Yuan L; Stefik M; Tang CB Designing Block Copolymer Architectures toward Tough Bioplastics from Natural Rosin. *Macromolecules* 2017, 50, 2069–2077; (c) Lin TP; Chang AB; Chen HY; Liberman-Martin AL; Bates CM; Voegtle MJ; Bauer CA; Grubbs RH Control of Grafting Density and Distribution in Graft Polymers by Living Ring-Opening Metathesis Copolymerization. *J. Am. Chem. Soc* 2017, 139, 3896–3903; [PubMed: 28221030] (d) Chang AB; Lin TP; Thompson NB; Luo SX; Liberman-Martin AL; Chen HY; Lee B; Grubbs RH Design, Synthesis, and Self-Assembly of Polymers with Tailored Graft Distributions. *J. Am. Chem. Soc* 2017, 139, 17683–17693; [PubMed: 29117478] (e) Neary WJ; Kennemur JG Variable Temperature ROMP: Leveraging Low Ring Strain Thermodynamics To Achieve Well-Defined Polypentenamers. *Macromolecules* 2017, 50, 4935–4941.
- (9). (a) Garber SB; Kingsbury JS; Gray BL; Hoveyda AH Efficient and recyclable monomeric and dendritic Ru-based metathesis catalysts. *J. Am. Chem. Soc* 2000, 122, 8168–8179; (b) Gessler S; Randl S; Blechert S Synthesis and metathesis reactions of a phosphine-free dihydroimidazole carbene ruthenium complex. *Tetrahedron Lett* 2000, 41, 9973–9976.
- (10). (a) Vidavsky Y; Anaby A; Lemcoff NG Chelating alkylidene ligands as pacifiers for ruthenium catalyzed olefin metathesis. *Dalton. Trans* 2012, 41, 32–43; [PubMed: 22020679] (b) Hoveyda AH; Gillingham DG; Van Veldhuizen JJ; Kataoka O; Garber SB; Kingsbury JS; Harrity JP Ru complexes bearing bidentate carbenes: from innocent curiosity to uniquely effective catalysts for olefin metathesis. *Org. Biomol. Chem* 2004, 2, 8–23. [PubMed: 14737653]
- (11). Vougioukalakis GC; Grubbs RH Ruthenium-based heterocyclic carbene-coordinated olefin metathesis catalysts. *Chem. Rev* 2010, 110, 1746–1787. [PubMed: 20000700]
- (12). (a) Sanford MS; Ulman M; Grubbs RH New Insights into the Mechanism of Ruthenium-Catalyzed Olefin Metathesis Reactions. *J. Am. Chem. Soc* 2001, 123, 749–750; [PubMed: 11456595] (b) Sanford MS; Love JA; Grubbs RH Mechanism and activity of ruthenium olefin metathesis catalysts. *J. Am. Chem. Soc* 2001, 123, 6543–6554; [PubMed: 11439041] (c) Wakamatsu H; Blechert S A new highly efficient ruthenium metathesis catalyst. *Angew. Chem. Int. Ed* 2002, 41, 2403–2405; (d) Shu C; Zeng X; Hao MH; Wei X; Yee NK; Busacca CA; Han Z; Farina V; Senanayake CH RCM macrocyclization made practical: an efficient synthesis of HCV protease inhibitor BILN 2061. *Org. Lett* 2008, 10, 1303–1306; [PubMed: 18293994] (e) Hejl A Controlling olefin metathesis through catalyst and monomer design. Ph.D. Thesis, California Institute of Technology, Pasadena, CA, 2007; (f) Bieniek M; Bujok R; Cabaj M; Lugan N; Lavigne G; Arlt D; Grela K Advanced fine-tuning of Grubbs/Hoveyda olefin metathesis catalysts: a further step toward an optimum balance between antinomic properties. *J. Am. Chem. Soc* 2006, 128, 13652–13653; [PubMed: 17044669] (g) Bieniek M; Samojlowicz C; Sashuk V; Bujok R; Sledz P; Lugan N; Lavigne G; Arlt D; Grela K Rational Design and Evaluation of Upgraded Grubbs/Hoveyda Olefin Metathesis Catalysts: Polyfunctional Benzyldiene Ethers on the Test Bench. *Organometallics* 2011, 30, 4144–4158; (h) Liberman-Martin AL; Grubbs RH Ruthenium Olefin Metathesis Catalysts Featuring a Labile Carbodicarbene Ligand. *Organometallics* 2017, 36, 4091–4094; (i) Czarnocki SJ; Czelusniak I; Olszewski TK; Malinska M; Wozniak K; Grela K Rational and Then Serendipitous Formation of Aza Analogues of Hoveyda-Type Catalysts Containing a Chelating Ester Group Leading to a Polymerization Catalyst Family. *ACS Catal* 2017, 7, 4115–4121.
- (13). (a) Vorfalt T; Wannowius KJ; Plenio H Probing the mechanism of olefin metathesis in Grubbs-Hoveyda and Grela type complexes. *Angew. Chem. Int. Ed* 2010, 49, 5533–5536; (b) Thiel V; Hendann M; Wannowius KJ; Plenio H On the mechanism of the initiation reaction in Grubbs-Hoveyda complexes. *J. Am. Chem. Soc* 2012, 134, 1104–1114; [PubMed: 22188483] (c) Nuñez-Zarur F; Solans-Monfort X; Rodríguez-Santiago L; Sodupe M Differences in the Activation Processes of Phosphine-Containing and Grubbs-Hoveyda-Type Alkene Metathesis Catalysts. *Organometallics* 2012, 31, 4203–4215; (d) Ashworth IW; Hillier IH; Nelson DJ; Percy JM; Vincent MA Olefin Metathesis by Grubbs-Hoveyda Complexes: Computational and Experimental Studies of the Mechanism and Substrate-Dependent Kinetics. *ACS Catal* 2013, 3,

1929–1939;(e)Bates JM; Lummiss JAM; Bailey GA; Fogg DE Operation of the Boomerang Mechanism in Olefin Metathesis Reactions Promoted by the Second-Generation Hoveyda Catalyst. *ACS Catal* 2014, 4, 2387–2394;(f)Nelson DJ; Manzini S; Urbina-Blanco CA; Nolan SP Key processes in ruthenium-catalysed olefin metathesis. *Chem. Commun* 2014, 50, 10355–10375;(g)Griffiths JR; Keister JB; Diver ST From Resting State to the Steady State: Mechanistic Studies of Ene-Yne Metathesis Promoted by the Hoveyda Complex. *J. Am. Chem. Soc* 2016, 138, 5380–5391. [PubMed: 27076098]

- (14). Engle KM; Lu G; Luo SX; Henling LM; Takase MK; Liu P; Houk KN; Grubbs RH Origins of initiation rate differences in ruthenium olefin metathesis catalysts containing chelating benzylidenes. *J. Am. Chem. Soc* 2015, 137, 5782–5792. [PubMed: 25897653]
- (15). (a)Barbasiewicz M; Bieniek M; Michrowska A; Szadkowska A; Makal A; Wozniak K; Grela K Probing of the ligand anatomy: Effects of the chelating alkoxy ligand modifications on the structure and catalytic activity of ruthenium carbene complexes. *Adv. Synth. Catal* 2007, 349, 193–203;(b)Sytniczuk A; Kajetanowicz A; Grela K Fishing for the right catalyst for the cross-metathesis reaction of methyl oleate with 2-methyl-2-butene. *Catal. Sci. Technol* 2017, 7, 1284–1296.
- (16). Kos P; Savka R; Plenio H Fast Olefin Metathesis: Synthesis of 2-Aryloxy-Substituted Hoveyda-Type Complexes and Application in Ring-Closing Metathesis. *Adv. Synth. Catal* 2013, 355, 439–447.
- (17). Bormand M; Torker S; Chen P Mechanistically designed dual-site catalysts for the alternating ROMP of norbornene and cyclooctene. *Organometallics* 2007, 26, 3585–3596.
- (18). (a)Bieszczad B; Barbasiewicz M The Key Role of the Nonchelating Conformation of the Benzylidene Ligand on the Formation and Initiation of Hoveyda–Grubbs Metathesis Catalysts. *Chem. Eur. J* 2015, 21, 10322–10325; [PubMed: 26074213] (b)Basak T; Grudzien K; Barbasiewicz M Remarkable Ability of the Benzylidene Ligand To Control Initiation of Hoveyda–Grubbs Metathesis Catalysts. *Eur. J. Inorg. Chem* 2016, 2016, 3513–3523.
- (19). Blum AP; Ritter T; Grubbs RH Synthesis of N-heterocyclic carbene-containing metal complexes from 2-(pentafluorophenyl)imidazolines. *Organometallics* 2007, 26, 2122–2124.
- (20). Stewart IC; Ung T; Pletnev AA; Berlin JM; Grubbs RH; Schrodi Y Highly efficient ruthenium catalysts for the formation of tetrasubstituted olefins via ring-closing metathesis. *Org. Lett* 2007, 9, 1589–1592. [PubMed: 17378575]
- (21). All of the computations were performed in the gas phase with Gaussian 09: Frisch MJ; Trucks GW; Schlegel HB; Scuseria GE; Robb MA; Cheeseman JR; Scalmani G; Barone V; Mennucci B; Petersson GA; Nakatsuji H; Caricato M; Li X; Hratchian HP; Izmaylov AF; Bloino J; Zheng G; Sonnenberg JL; Hada M; Ehara M; Toyota K; Fukuda R; Hasegawa J; Ishida M; Nakajima T; Honda Y; Kitao O; Nakai H; Vreven T; Montgomery JA Jr.; Peralta JE; Ogliaro F; Bearpark M; Heyd JJ; Brothers E; Kudin KN; Staroverov VN; Kobayashi R; Normand J; Raghavachari K; Rendell A; Burant JC; Iyengar SS; Tomasi J; Cossi M; Rega N; Millam JM; Klene M; Knox JE; Cross JB; Bakken V; Adamo C; Jaramillo J; Gomperts R; Stratmann RE; Yazyev O; Austin AJ; Cammi R; Pomelli C; Ochterski JW; Martin RL; Morokuma K; Zakrzewski VG; Voth GA; Salvador P; Dannenberg JJ; Dapprich S; Daniels AD; Farkas Ö; Foresman JB; Ortiz JV; Cioslowski J; Fox DJ Gaussian 09, revision D.01; Gaussian, Inc.: Wallingford, CT, 2009.
- (22). Trzaskowski B; Goddard WA; Grela K Faster initiating olefin metathesis catalysts from introducing double bonds into cyclopropyl, cyclobutyl and cyclopentyl derivatives of Hoveyda–Grubbs precatalysts. *Molecular Catalysis* 2017, 433, 313–320.
- (23). Engle KM; Luo SX; Grubbs RH An S_NAr approach to sterically hindered ortho-alkoxybenzaldehydes for the synthesis of olefin metathesis catalysts. *J. Org. Chem* 2015, 80, 4213–4220. [PubMed: 25826714]
- (24). CCDC 1825291 (16), 1825292 (17), 1825279 (18), 1825280 (19), 1825284 (20), 1825287 (21), 1825286 (22), 1825275 (23), 1825289 (24), 1825278 (25), 1825277 (26), 1825288 (27), 1825282 (28), 1825290 (32), 1825276 (33), 1825281 (34), 1825283 (35), 1825285 (37) and 1825293 (38) contain the supplementary crystallographic data for this paper. These data can be obtained free of charge from The Cambridge Crystallographic Data Centre.
- (25). (a)For examples of fast-initiating Grubbs–Hoveyda-type catalysts, see refs 12c, 12e, 14, 16 and the following: Grela K; Harutyunyan S; Michrowska A A highly efficient ruthenium catalyst for

metathesis reactions. *Angew. Chem. Int. Ed* 2002, 41, 4038–4040;(b)Clavier H; Caijo F; Borre E; Rix D; Boeda F; Nolan SP; Mauduit M Towards Long-Living Metathesis Catalysts by Tuning the N-Heterocyclic Carbene (NHC) Ligand on Trifluoroacetamide-Activated Boomerang Ru Complexes. *Eur. J. Org. Chem* 2009, 2009, 4254–4265;(c)Michrowska A; Bujok R; Harutyunyan S; Sashuk V; Dolgonos G; Grella K Nitro-substituted Hoveyda-Grubbs ruthenium carbenes: enhancement of catalyst activity through electronic activation. *J. Am. Chem. Soc* 2004, 126, 9318–9325; [PubMed: 15281822] (d)Zaja M; Connon SJ; Dunne AM; Rivard M; Buschmann N; Jiricek J; Blechert S Ruthenium olefin metathesis catalysts with modified styrene ethers: influence of steric and electronic effects. *Tetrahedron* 2003, 59, 6545–6558;(e)Zhan Z-YJ Ruthenium Complex Ligand, Ruthenium Complex, Carried Ruthenium Complex Catalyst and the Preparing Methods and the use thereof WO Patent 2007003135. 2007.

- (26). Nelson DJ; Queval P; Rouen M; Magrez M; Toupet L; Caijo F; Borre E; Laurent I; Crevisy C; Basle O; Mauduit M; Percy JM Synergic Effects Between N-Heterocyclic Carbene and Chelating Benzylidene-Ether Ligands Toward the Initiation Step of Hoveyda-Grubbs Type Ru Complexes. *ACS Catal* 2013, 3, 259–264.
- (27). There is a positive correlation between initiation rate and the benzylidene ¹H NMR shift. On the other hand, Ru–O bond length (as measured by X-ray crystallography) is found to be a comparatively poor predictor of initiation kinetics, except in cases where the Ru–O length is especially long. See Figures XX and XX in the Supporting Information for illustrative scatter plots.
- (28). (a)For theoretical description and examples of ¹H–¹H EXSY NMR studies, see: Jeener J; Meier BH; Bachmann P; Ernst RR Investigation of exchange processes by two-dimensional NMR spectroscopy. *J. Chem. Phys* 1979, 71, 4546–4553;(b)Johnston ER; Dellwo MJ; Hendrix J Quantitative 2d Exchange Spectroscopy Using Time-Proportional Phase Incrementation. *J. Magn. Reson* 1986, 66, 399–409;(c)Lu J; Ma DJ; Hu J; Tang WX; Zhu DX Nuclear magnetic resonance spectroscopic studies of pyridine methyl derivatives binding to cytochrome c. *J. Chem. Soc., Dalton Trans* 1998, 2267–2273;(d)Wenzel AG; Blake G; VanderVelde DG; Grubbs RH Characterization and dynamics of substituted ruthenacyclobutanes relevant to the olefin cross-metathesis reaction. *J. Am. Chem. Soc* 2011, 133, 6429–6439; [PubMed: 21452876] (e)MacMillan SN; Harman WH; Peters JC Facile Si-H bond activation and hydrosilylation catalysis mediated by a nickel-borane complex. *Chem. Sci* 2014, 5, 590–597.
- (29). Similar experiment was previously described in Ref. 12e. The data included here were collected independently, and the results are in overall good agreement with these previous findings.

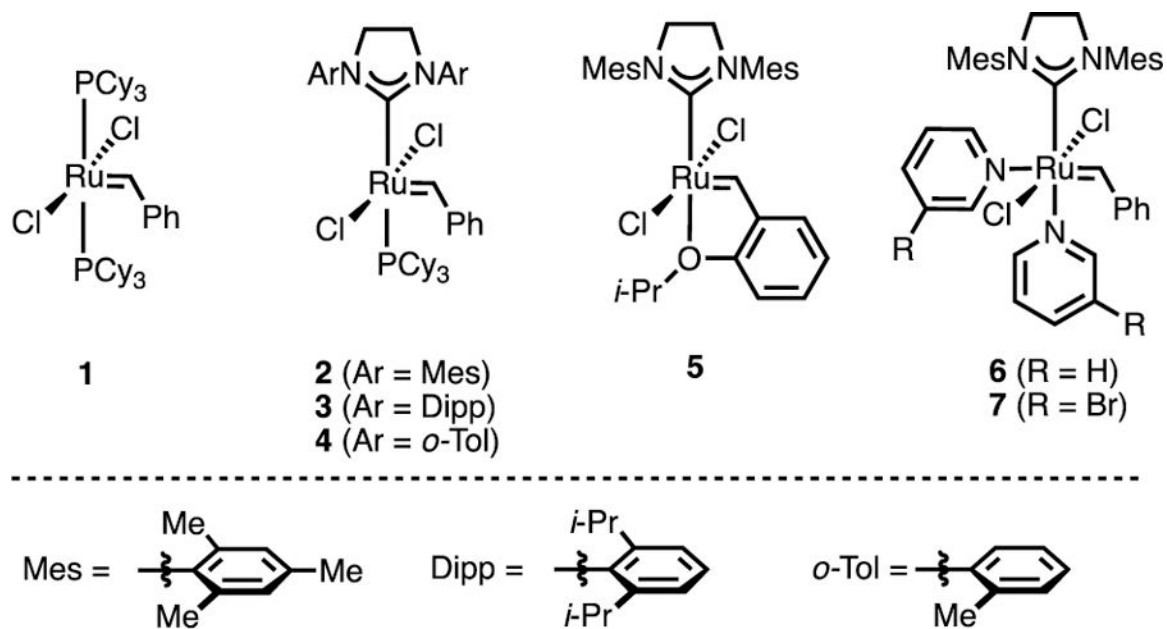


Figure 1. Commonly used ruthenium-based olefin metathesis catalysts.

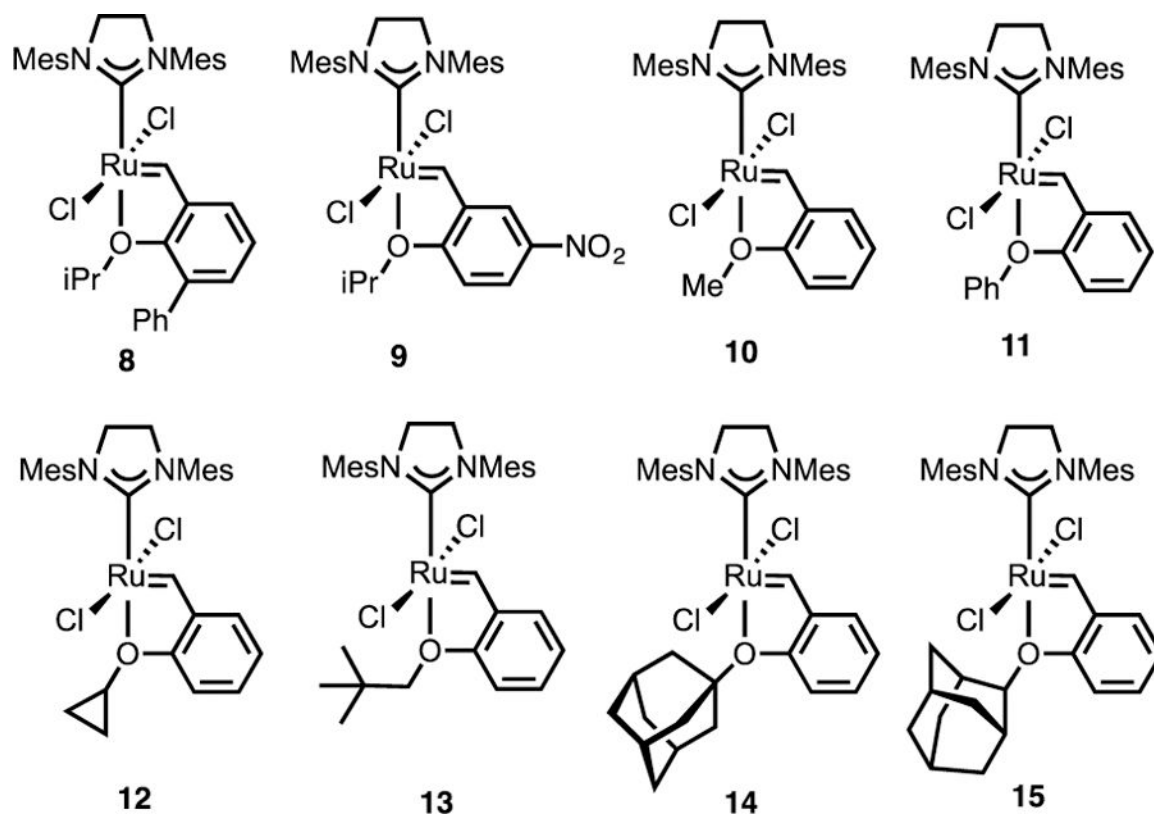
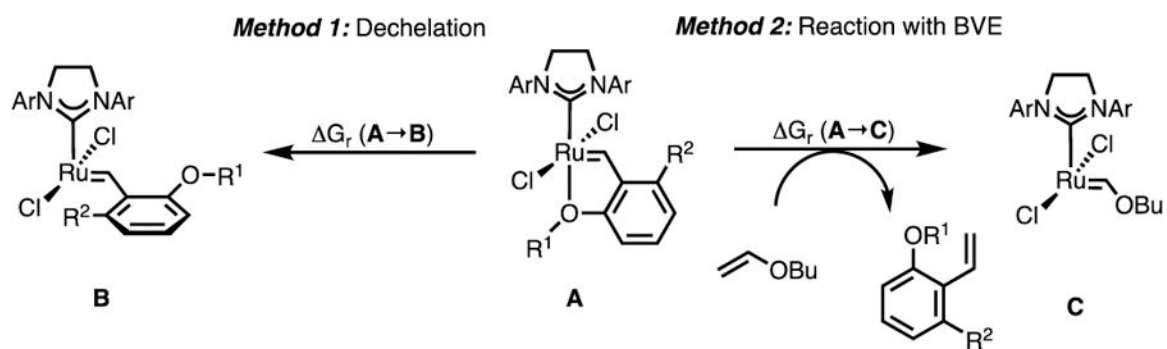


Figure 2.
Catalysts investigated previously with Hoveyda-type chelating benzylidenes (8–15).



$$\ln(k_{\text{obs}}) = -1.31(\Delta G_r(\mathbf{A} \rightarrow \mathbf{C})) + 6.97 \quad R^2 = 0.79 \quad (\text{Eq. 1})$$

k_{obs} : observed initiation rate (10^{-4} s^{-1})

$(\Delta G_r(\mathbf{A} \rightarrow \mathbf{C}) = \text{Ru-O bond strength } (\mathbf{A} \rightarrow \mathbf{C}) \text{ (kcal/mol)})$

Figure 3.
Computational model for catalyst initiation kinetics.

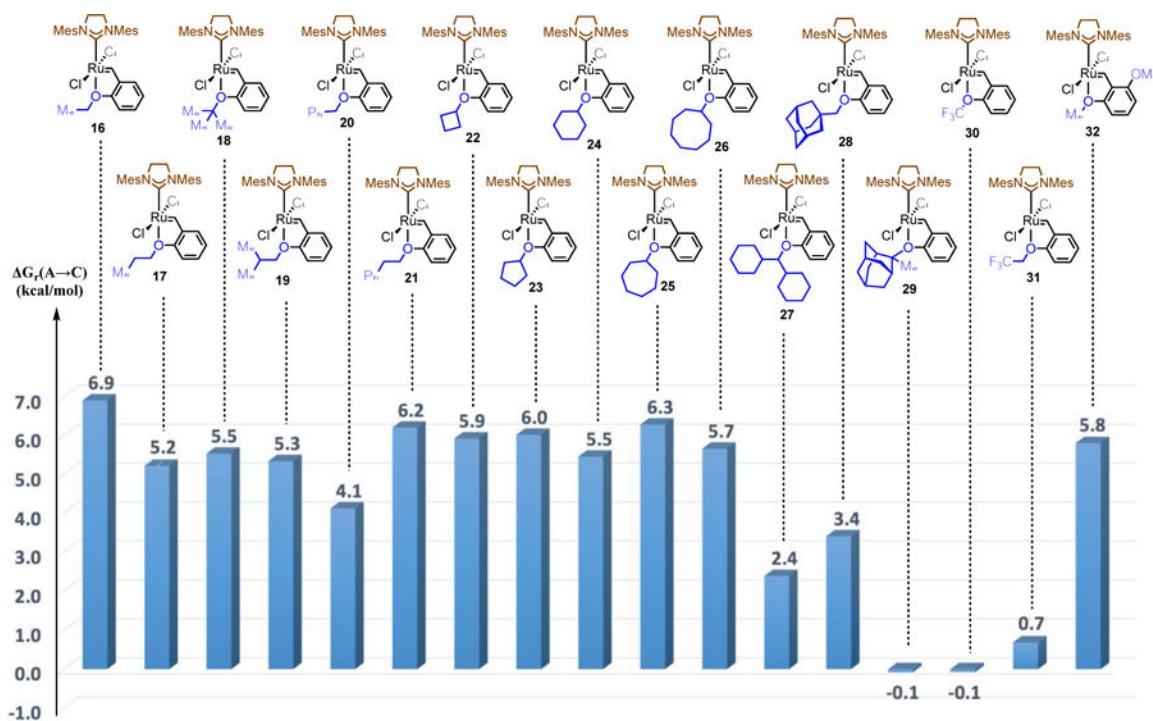


Figure 4. Computed Ru–O Bond Strengths ($G_r(\text{A} \rightarrow \text{C})$) for Representative SIMes Catalysts.

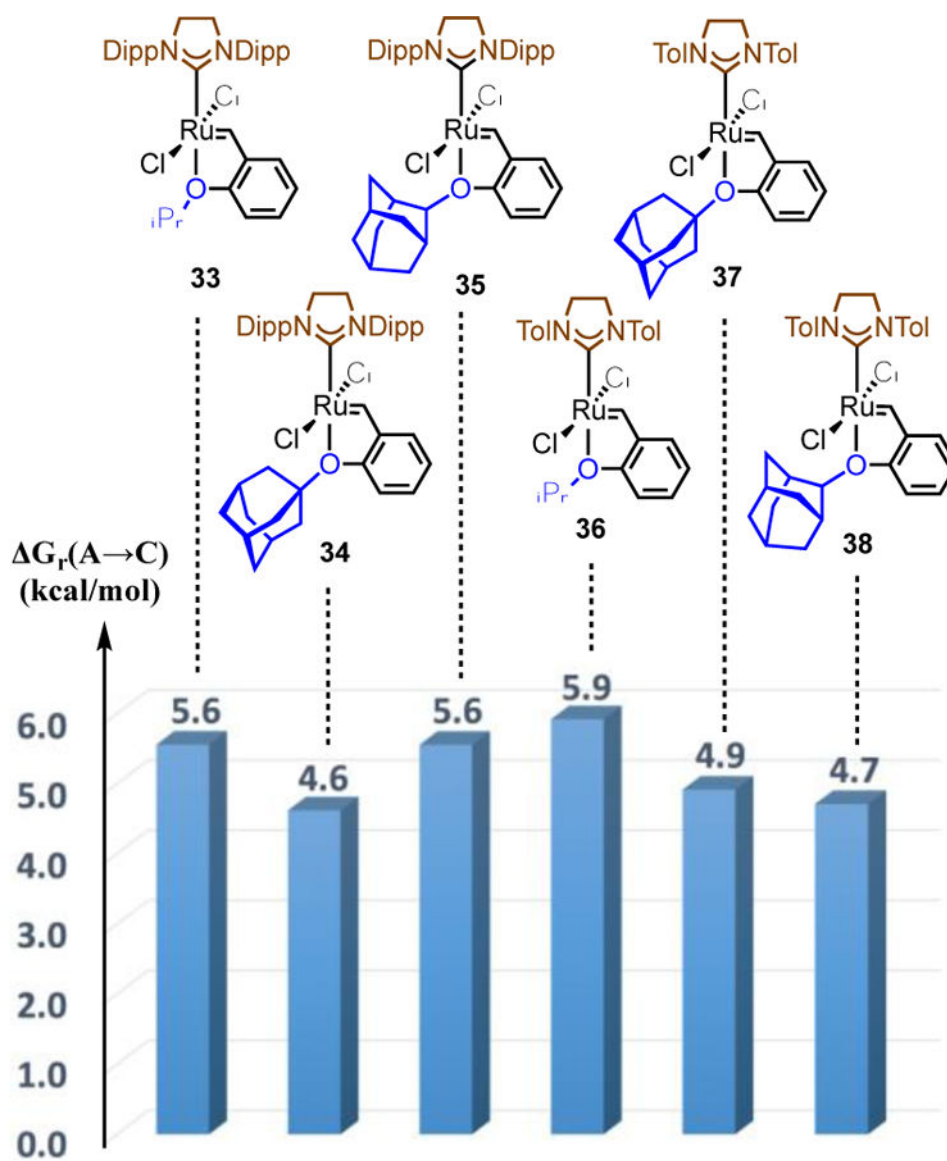


Figure 5.
Computed Ru-O Bond Strengths ($\Delta G_r(A \rightarrow C)$) for Non-SIMes Catalysts.

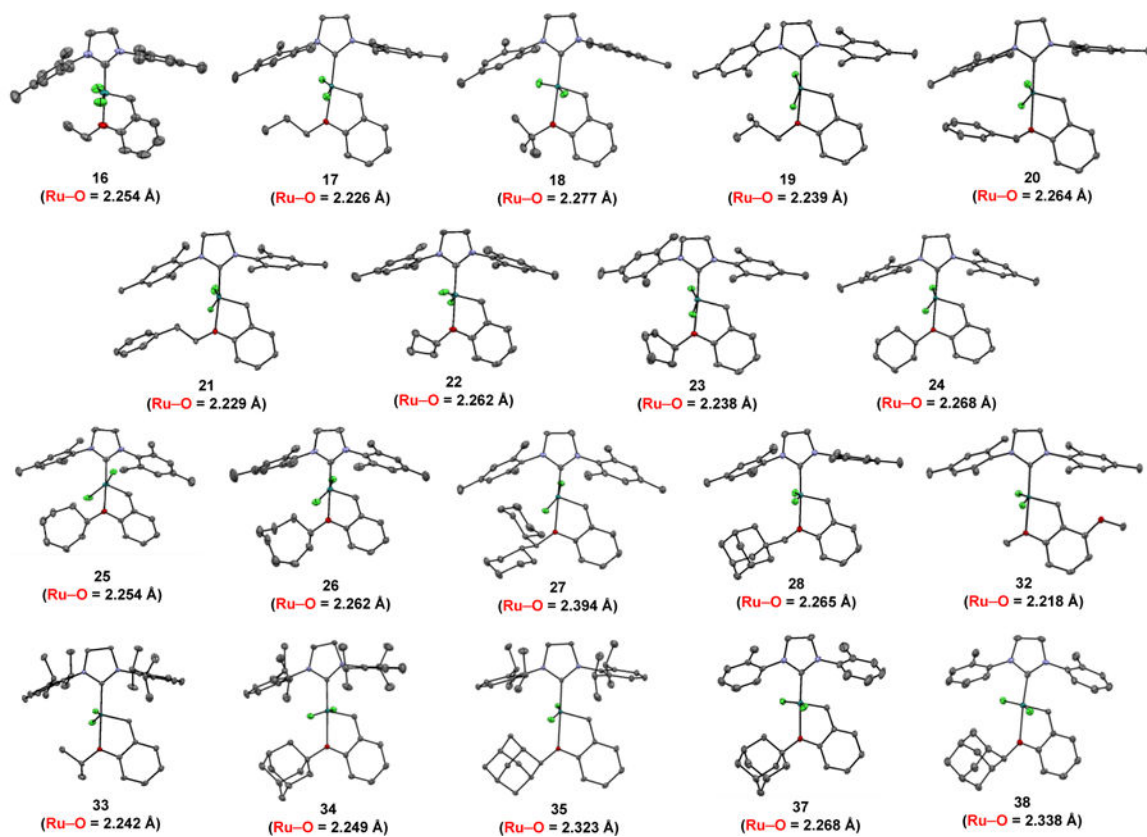


Figure 6.
Illustration of X-ray structures of the synthesized catalysts.

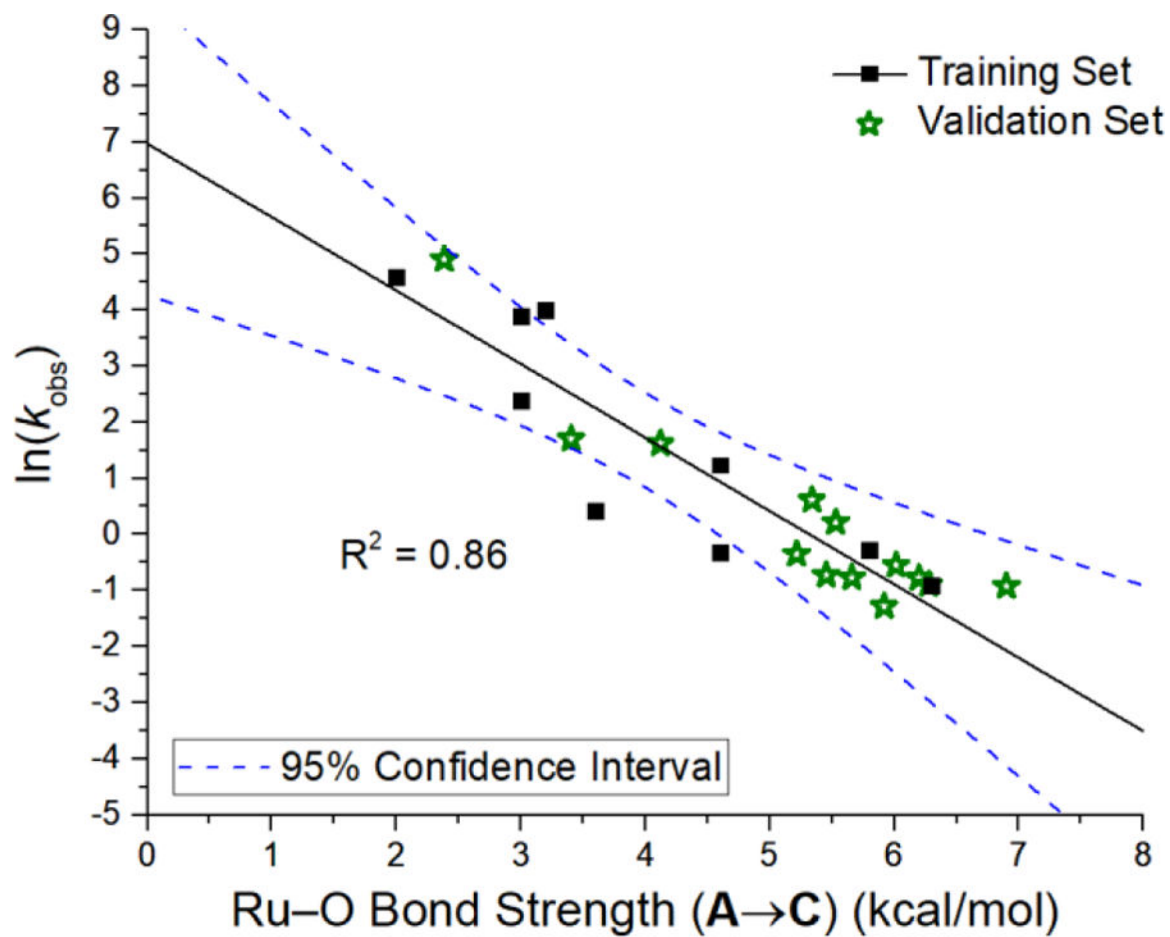


Figure 7. Validation of the initiation-prediction model results (SIMEs catalysts).

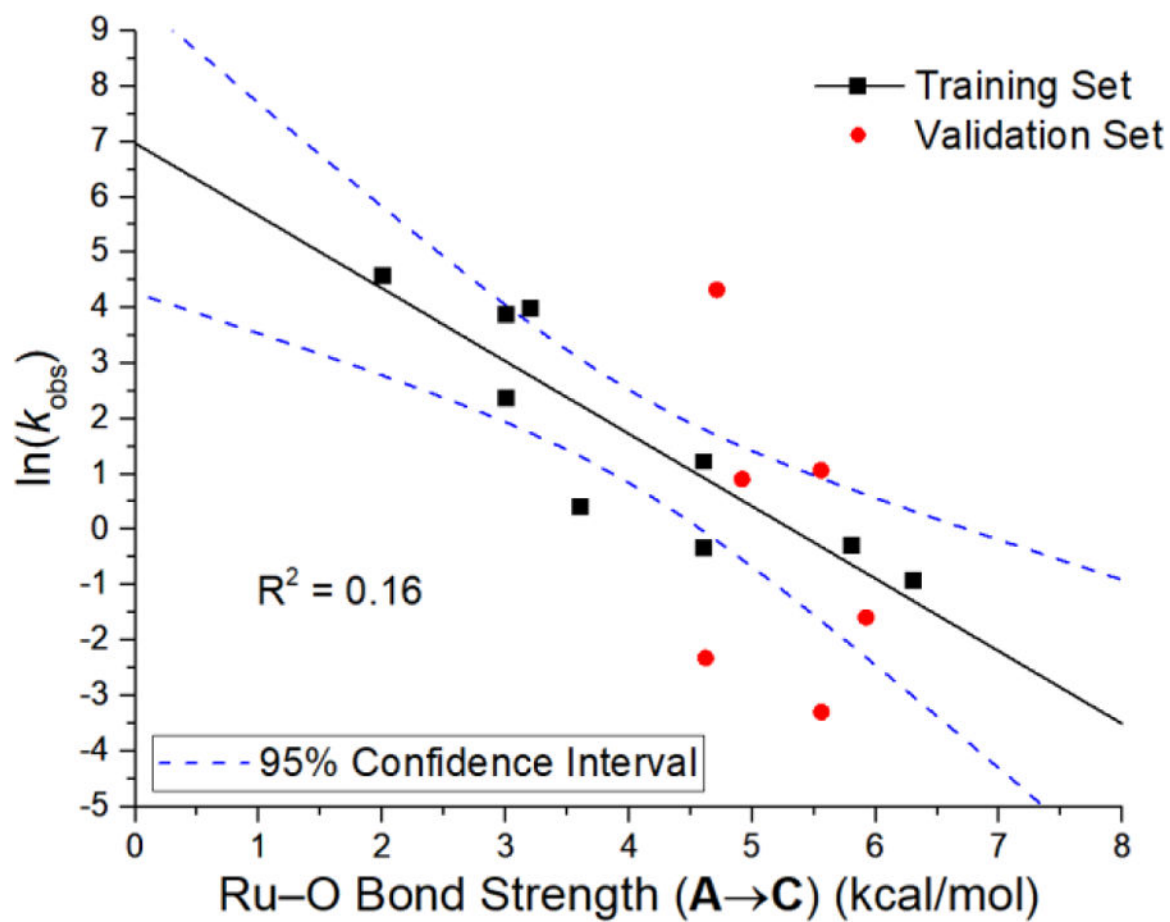


Figure 8. Validation of the initiation-prediction model results (SIPr and SITol catalysts).

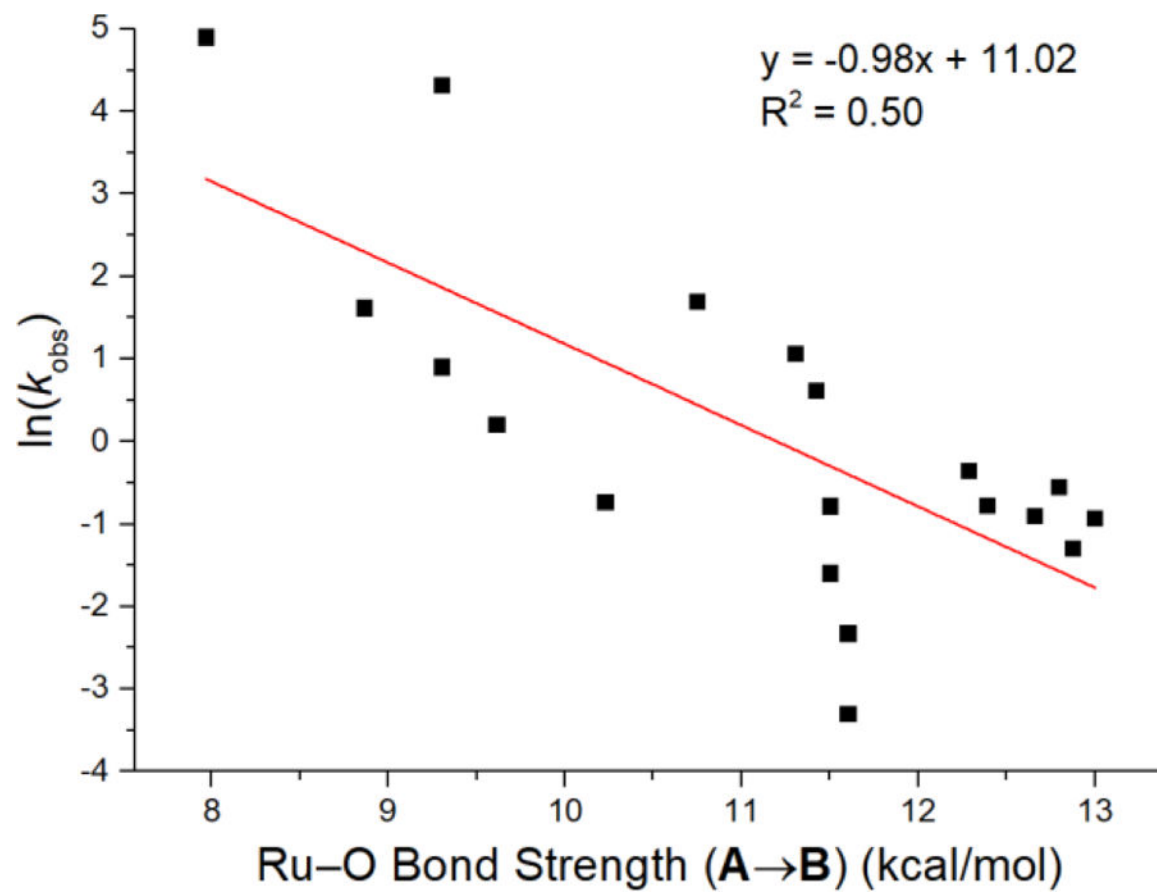


Figure 9.
 $\ln(k_{\text{obs}})$ versus Ru-O bond strength $G_{\text{r}}(\text{A} \rightarrow \text{B})$

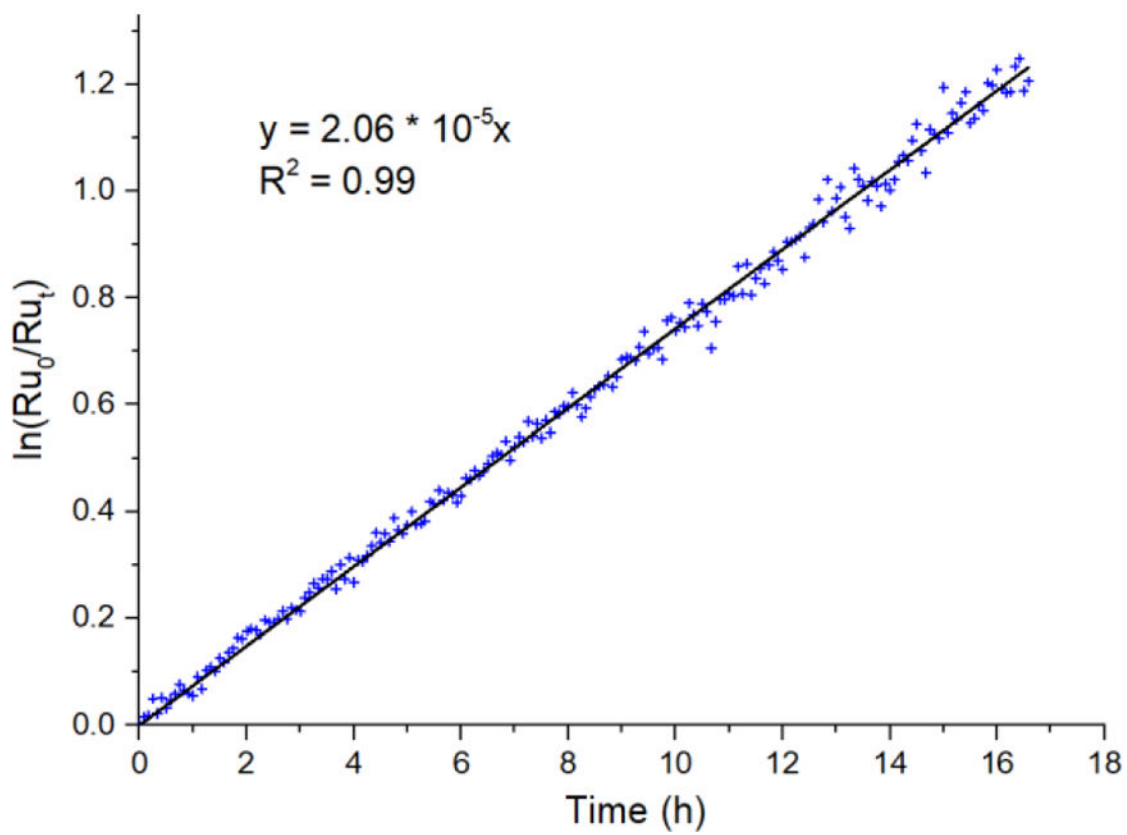
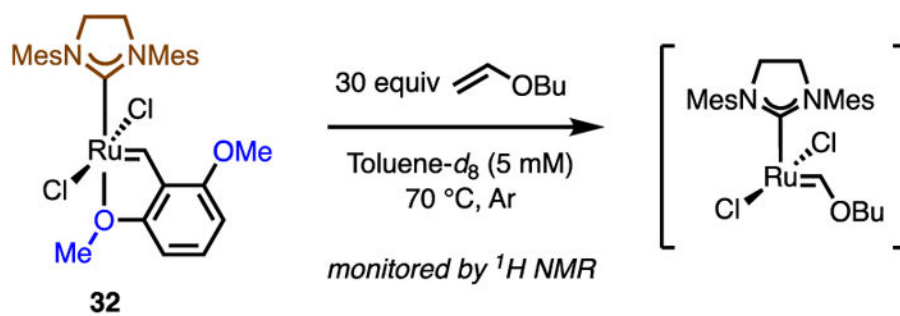


Figure 10. Initiation kinetics of catalyst **32** approximately over the course of two half-lives of the initiation reaction.

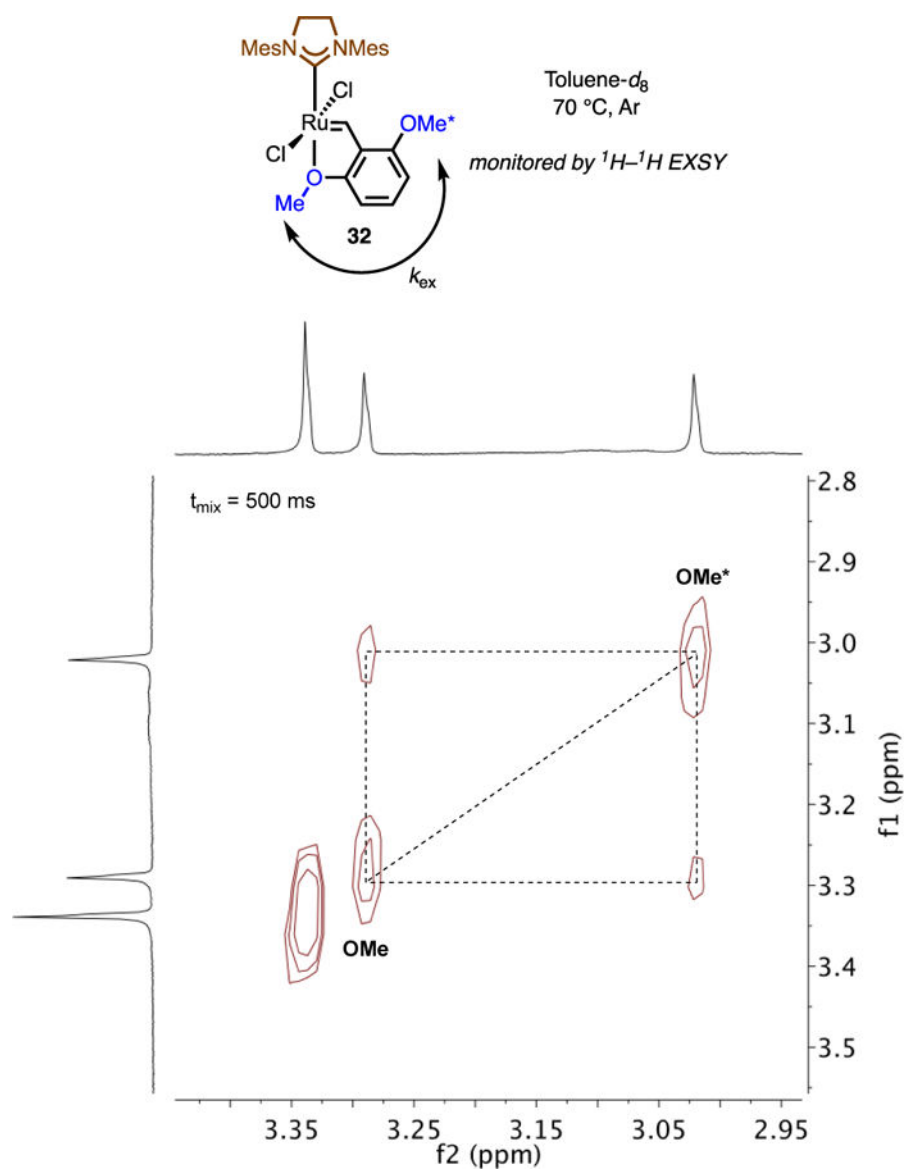
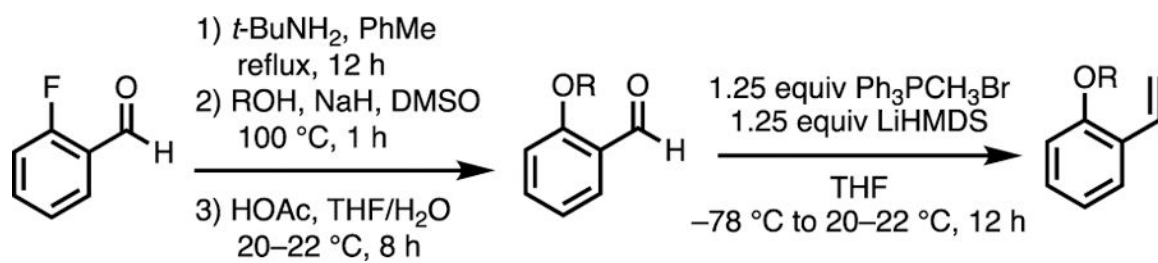


Figure 11. Representative ¹H-¹H EXSY spectrum for OMe exchange in **32** (*t*_{mix} = 500 ms)

**Scheme 1.**

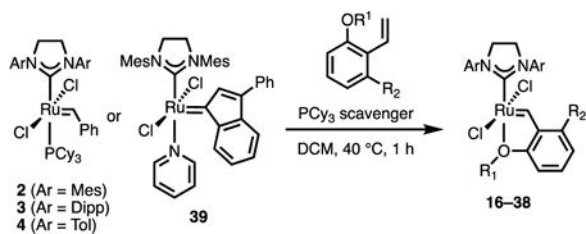
Synthesis of benzaldehyde intermediates and styrene chelates. ^aFor detailed procedures, see Supporting Information.

Table 1.

Computed Ru–O Bond Strengths and Predicted Initiation Rates.

entry	cat.	Ar =	R ¹ =	R ² =	G _r (A→B)	G _r (A→C)	Predicted Observed Initiation Rate ln(10 ⁻⁴ s ⁻¹)	ln(k _{obs})
1	5	Mes	<i>i</i> -Pr	H	12.8	6.3	-0.92 (expt.)	-2.07
2	16	Mes	Et	H	13.0	6.9		0.18
3	17	Mes	<i>n</i> -Pr	H	12.3	5.2		-0.28
4	18	Mes	<i>t</i> -Bu	H	9.6	5.5		0.02
5	19	Mes	<i>i</i> -Bu	H	11.4	5.3		1.57
6	20	Mes	Bn	H	8.9	4.1		-1.15
7	21	Mes	PhEt	H	11.5	6.2		-0.78
8	22	Mes	<i>c</i> -Bu	H	12.9	5.9		-0.91
9	23	Mes	<i>c</i> -Pentyl	H	12.8	6.0		-0.17
10	24	Mes	Cy	H	10.2	5.5		-1.25
11	25	Mes	<i>c</i> -Heptyl	H	12.7	6.3		-0.44
12	26	Mes	<i>c</i> -Octyl	H	12.4	5.7		3.85
13	27	Mes	CHC ₂	H	9.9	2.4		2.51
14	28	Mes	CH ₂ -1-Ada	H	10.7	3.4		7.07
15	29	Mes	2-Me-2-Ada	H	7.2	-0.1		7.06
16	30	Mes	CF ₃	H	6.8	-0.1		6.07
17	31	Mes	CH ₂ CF ₃	H	9.3	0.7		-0.60
18	32	Mes	Me	OMe	- ^a	5.8		-0.31
19	33	Dipp	<i>i</i> -Pr	H	11.6	5.6		0.92
20	34	Dipp	1-Ada	H	11.6	4.6		-0.31
21	35	Dipp	2-Ada	H	11.3	5.6		-0.79
22	36	<i>o</i> -Tol	<i>i</i> -Pr	H	11.5	5.9		0.53
23	37	<i>o</i> -Tol	1-Ada	H	9.3	4.9		0.80
24	38	<i>o</i> -Tol	2-Ada	H	9.3	4.7		

^a Calculation did not converge to a stable non-chelated 14 e⁻ complex. See Supporting Information for energy scan plot.

Table 2.Complexation attempts to prepare **16–32**, **34–35** and **37–38**.

entry	Ar =	R ¹ =	R ² =	cat.	Method	Yield
1	Mes	Et	H	16	A	51%
2	Mes	<i>n</i> -Pr	H	17	A	78%
3	Mes	<i>t</i> -Bu	H	18	A	91%
4	Mes	<i>i</i> -Bu	H	19	A	63%
5	Mes	Bn	H	20	A	58%
6	Mes	PhEt	H	21	A	85%
7	Mes	<i>c</i> -Bu	H	22	A	96%
8	Mes	<i>c</i> -Pentyl	H	23	A	95%
9	Mes	Cy	H	24	A	94%
10	Mes	<i>c</i> -Heptyl	H	25	A	98%
11	Mes	<i>c</i> -Octyl	H	26	A	77%
12	Mes	CHC ₂	H	27	A C	8% 47%
13	Mes	CH ₂ -1-Ada	H	28	B	54%
14	Mes	2-Me-2-Ada	H	29	-	0%
15	Mes	CF ₃	H	30	-	0%
16	Mes	CH ₂ -CF ₃	H	31	-	0%
17	Mes	Me	OMe	32	A B ^b	42% 55%
18	Dipp	1-Ada	H	34	B	64%
19	Dipp	2-Ada	H	35	B	42%
20	<i>o</i> -Tol	1-Ada	H	37	B	40%
21	<i>o</i> -Tol	2-Ada	H	38	B	33%

^aMethod A: **2** (0.2 mmol), styrene (0.2 mmol), and CuCl (0.2 mmol); Method B: **2/3/4** (0.2 mmol), styrene (0.4 mmol), and Amberlyst-15 (0.8 mmol); Method C: **39** (0.2 mmol), styrene (0.2 mmol), and Amberlyst-15 (0.8 mmol)

^bExtended reaction time (6 h). For detailed procedures, see Supporting Information.

Table 3.Summary of experimental Ru–O and Ru=C bond distances for catalysts **16–28** and **32–38**.

entry	cat.	R ¹ =	R ² =	R ³ =	Expt. (X-ray, Å) ^a	
					Ru–O	Ru=C
1	16	Mes	Et	H	2.254	1.818
2	17	Mes	<i>n</i> -Pr	H	2.226	1.832
3^b	18	Mes	<i>t</i> -Bu	H	2.277	1.828
4	19	Mes	<i>i</i> -Bu	H	2.239	1.832
5	20	Mes	Bn	H	2.264	1.831
6	21	Mes	PhEt	H	2.229	1.828
7^b	22	Mes	<i>c</i> -Bu	H	2.262	1.836
8	23	Mes	<i>c</i> -Pentyl	H	2.238	1.833
9	24	Mes	Cy	H	2.268	1.836
10	25	Mes	<i>c</i> -Heptyl	H	2.254	1.830
11^b	26	Mes	<i>c</i> -Octyl	H	2.262	1.842
12	27	Mes	CHCy ₂	H	2.394	1.821
13	28	Mes	CH ₂ -1-Ada	H	2.265	1.828
14	32	Mes	Methyl	MeO	2.218	1.839
15^b	33	Dipp	<i>i</i> -Propyl	H	2.242	1.832
16	34	Dipp	1-Ada	H	2.249	1.828
17	35	Dipp	2-Ada	H	2.323	1.829
18^c	36	<i>o</i> -Tol	<i>i</i> -Propyl	H	2.298	1.833
19	37	<i>o</i> -Tol	1-Ada	H	2.268	1.827
20	38	<i>o</i> -Tol	2-Ada	H	2.338	1.828

^aExperimental values are shown to three decimal places without estimated standard deviations for clarity. Estimated standard errors are typically in the range of 0.001–0.005 Å. See Supporting Information for additional details.

^bExperimental value represents the average of the two crystallographically inequivalent molecules found in the unit cell.

^cRef. 20.

Table 4.

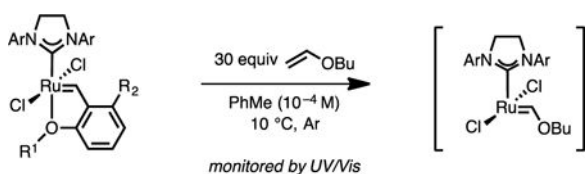
Diagnostic NMR peaks of the catalysts.

entry	cat	Ar =	R ¹ =	R ² =	Ru=CHAr		NHC
					¹ H	¹³ C	¹³ C
1	16	Mes	Et	H	16.52	294.71	211.58
2	17	Mes	<i>n</i> -Pr	H	16.52	295.23	211.53
3	18	Mes	<i>t</i> -Bu	H	16.50	298.91	211.77
4	19	Mes	<i>i</i> -Bu	H	16.57	296.08 ^c	210.81
5 ^b	20	Mes	Bn	H	16.55	290.80	209.83
6	21	Mes	PhEt	H	16.45	294.77	211.04
7	22	Mes	<i>c</i> -Bu	H	16.48	294.46 ^c	211.55
8	23	Mes	<i>c</i> -Pentyl	H	16.52	296.20 ^c	211.73
9	24	Mes	Cy	H	16.51	296.76 ^c	211.49
10	25	Mes	<i>c</i> -Heptyl	H	16.50	296.63 ^c	211.74
11	26	Mes	<i>c</i> -Octyl	H	16.51	296.44	211.21
12	27	Mes	CHCy ₂	H	16.72	296.60 ^c	208.83
13	28	Mes	CH ₂ -1-Ada	H	16.59	295.58 ^c	210.22
14 ^b	32	Mes	Methyl	OMe	17.25 ^d	286.02 ^c	211.18
15 ^b	33	Dipp	<i>i</i> -Pr	H	16.37	289.60 ^c	213.60
16	34	Dipp	1-Ada	H	16.43	294.83 ^c	214.67
17	35	Dipp	2-Ada	H	16.62	293.18 ^c	212.23
18 ^b	36	<i>o</i> -Tol	<i>i</i> -Propyl	H	16.47	295.21	210.89
19	37	<i>o</i> -Tol	1-Ada	H	16.39	297.91	211.54
20	38	<i>o</i> -Tol	2-Ada	H	16.57	296.26	209.09

^aSpectra in CD₂Cl₂^bThese values were independently measured and corresponded closely with the published values in the literature: entry 5 (Ref. 15a), entry 14 (Ref. 18a), entry 15 (Ref. 19) and entry 18 (Ref. 20).^cAverage of two or more peaks corresponding to the benzylidene NMR peak.^dBased on the major *trans* isomer.

Table 5.

Initiation rates of catalysts, displayed in increasing order for catalysts bearing the same NHC ligand.^{a,b}



entry	cat.	Ar =	R ¹ =	R ² =	λ_{\max}	k_{obs} (10^{-4} s^{-1})	k_{rel}
1	5	Mes	<i>i</i> -Pr	H	378	0.40 ± 0.04	1.0
2	32	Mes	Me	OMe	376	- ^c	-
3	22	Mes	<i>c</i> -Butyl	H	378	0.28 ± 0.02	0.7
4	16	Mes	Et	H	376	0.40 ± 0.04	1.0
5	25	Mes	<i>c</i> -Heptyl	H	380	0.41 ± 0.03	1.0
6	21	Mes	PhEt	H	376	0.46 ± 0.07	1.1
7	26	Mes	<i>c</i> -Octyl	H	380	0.46 ± 0.01	1.2
8	24	Mes	Cy	H	380	0.48 ± 0.06	1.2
9	23	Mes	<i>c</i> -Pentyl	H	380	0.58 ± 0.04	1.4
10	17	Mes	<i>n</i> -Pr	H	376	0.71 ± 0.02	1.8
11	18	Mes	<i>t</i> -Bu	H	380	1.24 ± 0.04	3.1
12	19	Mes	<i>i</i> -Bu	H	378	1.85 ± 0.06	4.6
13	20	Mes	Bn	H	370	5.07 ± 0.62	13
14	28	Mes	CH ₂ -1-Ada	H	374	5.50 ± 0.37	14
15	27	Mes	CHCy ₂	H	376	135 ± 4.24	340
16	33	Dipp	<i>i</i> -Pr	H	374	0.04 ^d	0.1
17	34	Dipp	1-Ada	H	378	0.10 ^d	0.3
18	35	Dipp	2-Ada	H	378	2.91 ± 0.09	7.3
19	36	<i>o</i> -Tol	<i>i</i> -Pr	H	374	0.20 ± 0.06	0.5
20	37	<i>o</i> -Tol	1-Ada	H	378	2.48 ± 0.31	6.2
21	38	<i>o</i> -Tol	2-Ada	H	376	75.5 ± 8.94	190




^aThe k_{obs} values are reported as averages (with 95% confidence intervals) determined from three independent trials.

^bThe relative rate (k_{rel}) was calculated by dividing the k_{obs} value of the catalyst of interest by the k_{obs} value for catalyst 5.

^cCatalyst 32 was found not to initiate at 10 °C.

^dDue to the slow initiation kinetics, the k_{obs} values were determined from a single trial.

Table 6.Effect of NHC ligand variations on initiation rates.^a

Alkoxy \ NHC	SIPr 	SIMes 	SITol 
<i>i</i>-Pr	$k_{\text{rel}} = 1.0$ (33)	$k_{\text{rel}} = 11$ (5)	$k_{\text{rel}} = 5.5$ (36)
1-Ada	$k_{\text{rel}} = 2.6$ (34)	$k_{\text{rel}} = 94$ (14)	$k_{\text{rel}} = 67$ (37)
2-Ada	$k_{\text{rel}} = 79$ (35)	$k_{\text{rel}} = 1500$ (15)	$k_{\text{rel}} = 2000$ (38)

^aThe relative rate (k_{rel}) was calculated by dividing the k_{Obs} value of the catalyst of interest by the k_{Obs} value for catalyst **33**.

Table 7.

Comparison between predicted and experimental initiation rates

entry	cat.	Ar =	R ¹ =	R ² =	Predicted	Experimental
					$\frac{\ln(k_{\text{obs}})}{\ln(10^{-4} \text{ s}^{-1})}$	$\frac{\ln(k_{\text{obs}})}{\ln(10^{-4} \text{ s}^{-1})}$
1	22	Mes	<i>c</i> -Butyl	H	-0.78	-1.28
2	16	Mes	Et	H	-2.07	-0.93
3	25	Mes	<i>c</i> -Heptyl	H	-1.25	-0.90
4	21	Mes	PhEt	H	-1.15	-0.78
5	26	Mes	<i>c</i> -Octyl	H	-0.44	-0.77
6	24	Mes	Cy	H	-0.17	-0.73
7	23	Mes	<i>c</i> -Pentyl	H	-0.91	-0.55
8	17	Mes	<i>n</i> -Pr	H	0.14	-0.35
9	18	Mes	<i>t</i> -Bu	H	-0.28	0.22
10	19	Mes	<i>i</i> -Bu	H	0.02	0.62
11	20	Mes	Bn	H	1.57	1.62
12	28	Mes	CH ₂ -1-Ada	H	2.51	1.70
13	27	Mes	CHCy ₂	H	3.85	4.91
14	33	Dipp	<i>i</i> -Pr	H	-0.31	-3.30
15	34	Dipp	1-Ada	H	0.92	-2.32
16	35	Dipp	2-Ada	H	-0.31	1.07
17	36	<i>o</i> -Tol	<i>i</i> -Pr	H	-0.79	-1.59
18	37	<i>o</i> -Tol	1-Ada	H	0.53	0.91
19	38	<i>o</i> -Tol	2-Ada	H	0.80	4.32

Table 8.Comparison of OMe exchange and interchange rate of **32**

process	k (10^{-3} s^{-1})	T ($^{\circ}\text{C}$)	rel. rate
OMe exchange	450	70	3300
Interchange with BVE	0.14	70	1

Author Manuscript

Author Manuscript

Author Manuscript

Author Manuscript